Phonon-assisted heat transfer between vacuum-separated surfaces

J. B. Pendry,[1] K. Sasihithlu,[1] and R. V. Craster[2]
[1]*The Blackett Laboratory, Department of Physics, Imperial College London, London SW7 2AZ, UK*
[2]*Department of Mathematics, Imperial College London, London SW7 2AZ, UK*
(Received 11 May 2016; revised manuscript received 15 July 2016; published 11 August 2016)

With increasing interest in nanotechnology, the question arises of how heat is exchanged between materials separated by only a few nanometers of vacuum. Here, we present calculations of the contribution of phonons to heat transfer mediated by van der Waals forces and compare the results to other mechanisms such as coupling through near field fluctuations. Our results show a more dramatic decay with separation than previous work.

DOI: 10.1103/PhysRevB.94.075414

I. INTRODUCTION

Several recent papers have proposed that phonons may contribute to the transfer of heat between two closely spaced materials [1–4], but estimates differ in how large an effect is to be expected. Here, we make an investigation based on a realistic phonon spectrum and a careful calculation of the van der Waals forces that can transfer phonons from one surface to another across the vacuum.

It has long been recognized that when two materials are in close proximity *in vacuo*, their exchange of heat is no longer dictated by thermal radiation [5–8]. For a more complete set of references to earlier work, see Refs. [7,9]. Once closer than the typical wavelength of radiation, other near field mechanisms come into play. These are the same thermal fluctuations that give rise to Johnson noise in resistors: Their fluctuations are on a length scale reaching down to atomic level, but they are confined to the vicinity of the surface. Depending on the conductivity of the material, near field heat transfer can be by far the dominant term for surfaces in close proximity.

On the other hand, most of the heat content of a solid lies in the phonon spectrum, and more recent papers [1–4] raise the possibility that phonons may tunnel across the vacuum from one surface to another, mediated by van der Waals forces. Budaev and Bogy [2] were one of the first to investigate this possibility and gave estimates that suggested the phonon contribution could be large. However, more recently Ezzahri and Joulain [3] gave much smaller estimates of phonon heat transfer. In this paper, we present a model of the phonons and the van der Waals transfer mechanism, which depends much more strongly on separation than indicated in previous reports. We also suggest another mechanism for phonon tunneling based on electrostatic potential differences between surfaces, and we compare phonon heat transfer with the near field mechanism.

II. PHONONS IN SOLIDS

We shall assume an isotropic material that sustains longitudinal and transverse phonons. The longitudinal phonons have displacements parallel to the direction of propagation.

$$\mathbf{u}_L = k_L^{-1}[k_{Lx},\, k_y,\, 0]\exp(ik_{Lx}x + ik_y y - i\omega t) \tag{1}$$

and transverse phonons displacements perpendicular to that direction. There are two transverse phonons.

$$\mathbf{u}_{T1} = k_T^{-1}[k_y,\ -k_{Tx},\, 0]\exp(ik_{Tx,}x + ik_y y - i\omega t),$$
$$\mathbf{u}_{T2} = k_T^{-1}[0,\, 0,\, k_T]\exp(ik_{Tx,}x + ik_y y - i\omega t) \tag{2}$$

We shall assume a surface for which the normal is the x axis. Since we also assume an isotropic medium, we can work in the xy plane without loss of generality.

When we consider interaction of these phonons with a surface, only the p-polarized transverse wave, $\mathbf{u}_{T1}$, produces disturbances of the surface, and therefore it is only this wave that will transmit energy across a gap to a second surface. This wave is sometimes also referred to as a "vertical transverse wave."

The dynamics of the phonons are determined by the strain tensor,

$$u_{ik} = \frac{1}{2}\left[\frac{\partial u_i}{\partial x_k} + \frac{\partial u_k}{\partial x_i}\right] \tag{3}$$

and by the stress tensor,

$$\sigma_{ik} = \rho c_L^2 \delta_{ik}\sum_\ell u_{\ell\ell} + 2\rho c_T^2\left(u_{ik} - \delta_{ik}\sum_\ell u_{\ell\ell}\right) \tag{4}$$

where c_L is the velocity of longitudinal phonons, and c_T is the velocity of transverse phonons. Details can be found in Landau and Lifshitz [10].

Continuum theory relates the acceleration of an infinitesimal region of the medium to the gradient of the stress,

$$\rho\ddot{u}_x = \frac{\partial \sigma_{xx}}{\partial x} = -c_L^2 k_{Lx}^2 \exp\left(ik_{Lx}x - i\omega t\right) \tag{5}$$

in the case of longitudinal phonons and

$$\rho\ddot{u}_y = \frac{\partial \sigma_{yx}}{\partial x} = -c_T^2 k_{Tx}^2 \exp\left(ik_{Tx}x - i\omega t\right) \tag{6}$$

in the case of transverse phonons.

In reality, solids are composed of discrete unit cells that result in a cutoff to the wave vectors and a dispersion of frequency with wave vector, which can be quite complex but is typically of the form

$$\omega_{L,T}(k) = \omega_{c,L,T}\sin ak \tag{7}$$

where for a simple cubic lattice of atoms, a would be the lattice spacing, and the critical frequency would be given by

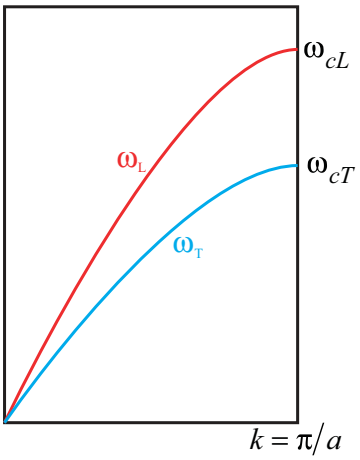

FIG. 1. Typical dispersion of phonon frequencies with wave vector.

the relevant velocity,

$$\lim_{k\to 0}\frac{d\omega_{L,T}}{dk} = c_{L,T} = \omega_{c,L,T}\, a \tag{8}$$

In a finite solid containing L^3 atoms, the first Brillouin zone contains L^3 phonons for each of the three modes. In our model, we replace the first Brillouin zone with a sphere of the same volume in reciprocal space. The radius is given by

$$\frac{4\pi}{3}k_c^3 = \left[\frac{2\pi}{a}\right]^3 \tag{9}$$

This leaves us with an isotropic continuum model, but one that captures the essential features of phonons in the solid state. Qualitative dispersion relations are shown in Fig. 1. The transverse wave typically has a larger wave vector at a given frequency and hence a lower cutoff frequency than the longitudinal phonon. However, we shall approximate the dispersion by linearizing, e.g., Eq. (7), as small values of the wave vector will dominate heat transfer.

III. VAN DER WAALS FORCES BETWEEN SURFACES

The van der Waals force originates from quantum fluctuations in electron density. It is a weak but relatively long range force that comes into its own at distances beyond the range of ordinary chemical bonds and is important for issues such as friction and wetting of surfaces. More esoterically, it enables geckos to walk on ceilings. It is well described by Israelachvili [11].

The van der Waals force acts on density fluctuations so that phonons with zero or negligible density fluctuations in the bulk have no bulk contributions to the force. However, all phonons (except for the transverse phonons at normal incidence) have a surface displacement, which does couple. This statement is true of the transverse phonons, which do not compress the material in the bulk, and is approximately true of the longitudinal phonons.

Suppose that surface 1 has a periodic displacement of

$$u_{1x} = \delta_{1x}\exp(ik_y y - i\omega t) \tag{10}$$

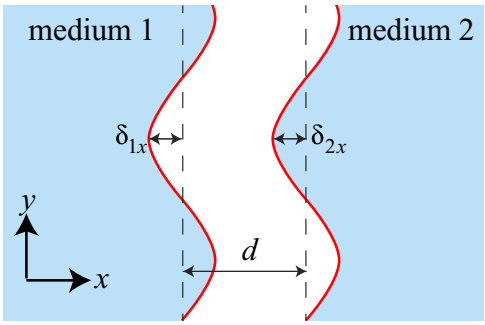

FIG. 2. Infinitesimal displacements of medium 1 and medium 2 alter the density profile at each surface. Thus, a periodic force is transmitted across the vacuum via the van der Waals interaction.

where δ_{1x} is an infinitesimal amplitude. From the translational symmetry of the surfaces, the force acting on surface 2 must have the form

$$F_{x21}\exp(ik_y y - i\omega t) \tag{11}$$

We consider the real and imaginary parts of the displacement separately, recombining them later. Here is the real part of the displacement:

$$u_{1x}^c = \delta_{1x}\cos(k_y y - \omega t) \tag{12}$$

To find the force acting on surface 2, we make a test displacement of surface 2 as follows,

$$u_{2x}^c = \delta_{2x}\cos(k_y y - \omega t) \tag{13}$$

This displacement changes the density at the surface by an infinitesimal amount,

$$\begin{aligned}\Delta\rho_1 &= \rho\delta_{1x}\cos(k_y y - \omega t)\delta(x)\\ \Delta\rho_2 &= -\rho\delta_{2x}\cos(k_y y - \omega t)\delta(x-d)\end{aligned} \tag{14}$$

where ρ is the density of the medium (see Fig. 2). Note the change of sign: A positive displacement on the first surface increases the density by pushing out into the vacuum, whereas a positive displacement on the second surface reduces the density by pushing material away from the vacuum.

The van der Waals potential energy in the presence of displacements is given by

$$\begin{aligned}\phi = \phi_0 + \phi_1 + \phi_2 = -C\iint_{R_0}\frac{d^3\mathbf{r}_1\, d^3\mathbf{r}_2}{|\mathbf{r}_1-\mathbf{r}_2|^6}\\ -C\iint_{R_1}\frac{d^3\mathbf{r}_1\, d^3\mathbf{r}_2}{|\mathbf{r}_1-\mathbf{r}_2|^6} - C\iint_{R_2}\frac{d^3\mathbf{r}_1\, d^3\mathbf{r}_2}{|\mathbf{r}_1-\mathbf{r}_2|^6}\end{aligned} \tag{15}$$

where ϕ_0 is the potential interaction between two undisturbed surfaces separated by distance d and represents the constant van der Waals attraction between the surfaces. It plays no role in transmitting phonons. On the other hand, ϕ_1 is the interaction between the perturbation on surface 1 and a planar undisturbed surface 2 plus the corresponding term where surface 2 is disturbed. The term $\mathbf{r}_1$ is a coordinate within the first surface (Fig. 2), and $\mathbf{r}_2$ is a coordinate within the second surface. Since the integrand oscillates about zero in y, the net contribution to the integral is zero to first order but has a second-order

contribution of

$$\phi_1 = -\frac{\pi C}{8d^4} L^2 \left(\delta_{1x}^2 + \delta_{2x}^2\right) \tag{16}$$

which gives rise to forces per unit area of

$$F_{x11}^c = \frac{\pi C \delta_{1x}}{2d^4} \cos(k_y y_1), \quad F_{x22}^c = \frac{\pi C \delta_{2x}}{2d^4} \cos(k_y y_1) \tag{17}$$

The constant C is proportional to the Hamaker constant, A [11],

$$C = A\pi^{-2} \tag{18}$$

We are left with ϕ_2, which is the interaction between the periodic displacements on each surface.

$$\phi_2 = +C \iint_{R_2} \frac{u_{1x}^c(\mathbf{r}_1) u_{2x}^c(\mathbf{r}_2) d^2\mathbf{r}_1 d^2\mathbf{r}_2}{|\mathbf{r}_1 - \mathbf{r}_2|^6} \tag{19}$$

where we have assumed that the displacements normal to the surface are infinitesimal.

Substituting for u_{1x}, u_{2x},

$$\begin{aligned}\phi_2 &= +C\delta_{1x}\delta_{2x} \iint_{R_2} \frac{\cos[k_y y_1 - \omega t]\cos[k_y y_2 - \omega t]}{|\mathbf{r}_1 - \mathbf{r}_2|^6} d^2\mathbf{r}_1 d^2\mathbf{r}_2 \\ &= +\frac{C\delta_{1x}\delta_{2x}}{2} \iint_{R_2} \frac{\cos[k_y(y_1 - y_2)]}{|\mathbf{r}_1 - \mathbf{r}_2|^6} d^2\mathbf{r}_1 d^2\mathbf{r}_2 \end{aligned} \tag{20}$$

Introducing new variables,

$$\mathbf{R} = \frac{\mathbf{r}_1 + \mathbf{r}_2}{2}, \quad \mathbf{r} = \mathbf{r}_1 - \mathbf{r}_2 - \mathbf{d} \tag{21}$$

gives

$$\begin{aligned}\phi_2 &= \frac{C\delta_{1x}\delta_{2x}L^2}{2} \iint_{R_2} \frac{\cos[k_y y]}{|\mathbf{r} + \mathbf{d}|^2} d^2\mathbf{r} \\ &= \frac{C\delta_{1x}\delta_{2x}L^2}{2} \mathrm{Re} \iint_{R_2} \frac{\exp[ik_y y]}{|\mathbf{r} + \mathbf{d}|^2} d^2\mathbf{r} \end{aligned} \tag{22}$$

where L^2 is the surface area of the interface and results from integrating over $\mathbf{R}$. This integral can be evaluated in terms of a modified Bessel function [12].

$$\phi_2 = \frac{CL^2\pi\delta_{1x}\delta_{2x}}{8d^2} k_y^2 K_2(k_y d) \tag{23}$$

This result has been exploited in the context of ^{4}He scattering from a liquid ^{4}He surface, where the experiment was dominated by the excitation of ripplons on the ^{4}He surface [13,14].

We can now retrieve the force per unit area acting on the second surface, due to a displacement of surface 1,

$$F_{x21}^c = -L^{-2} \frac{\partial \phi_2}{\partial \delta_{2x}} = -\frac{C\pi\delta_{1x}}{4d^2} k_y^2 K_2(k_y d) \tag{24}$$

If the displacements are infinitesimal, no shear force is transmitted across the vacuum,

$$F_{y21} e^{(ik_y y - i\omega t)} = 0 \tag{25}$$

A parallel argument holds for the imaginary component of the force, so that we identify

$$\begin{aligned} F_{x21} e^{(ik_y y - i\omega t)} &= -\frac{C\pi\delta_{1x}}{4d^2} k_y^2 K_2(k_y d) e^{(ik_y y - i\omega t)} \\ F_{y21} e^{(ik_y y - i\omega t)} &= 0 \end{aligned} \tag{26}$$

The forces exerted on surface 1 due to a displacement of surface 2 follow from symmetry,

$$\begin{aligned} F_{x12} e^{(ik_y y - i\omega t)} &= -\frac{C\pi\delta_{2x}}{4d^2} k_y^2 K_2(k_y d) e^{(ik_y y - i\omega t)} \\ F_{y12} e^{(ik_y y - i\omega t)} &= 0 \end{aligned} \tag{27}$$

Note that in the limit $d \to 0$, we retrieve the same functional form used in the "spring model" of previous work [2,3],

$$\begin{aligned} &\lim_{d\to 0} [\phi_1 + \phi_2] \\ &= \lim_{d\to 0} CL^2 \left[-\frac{\pi}{8d^4}\left(\delta_{1x}^2 + \delta_{2x}^2\right) + \frac{\pi\delta_{1x}\delta_{2x}}{8d^2} k_y^2 K_2(k_y d) \right] \\ &= -\frac{\pi CL^2}{8d^4}\left[\delta_{1x}^2 + \delta_{2x}^2 - 2\delta_{1x}\delta_{2x}\right] = -\frac{\pi CL^2}{8d^4}[\delta_{1x} - \delta_{2x}]^2 \end{aligned} \tag{28}$$

In this limit, the forces are a function only of the local separation of the surfaces. However, this limit is valid only at unrealistically small values of d.

IV. PHONON TRANSMISSION BETWEEN FREE SURFACES

We shall assume an isotropic material that sustains longitudinal and transverse phonons as defined in Eqs. (1)–(4). We wish to calculate the transmission coefficient for phonons incident on surface 1 separated by vacuum from surface 2 by a distance d (see Fig. 3).

First consider the case of an incident longitudinal phonon: Displacements are given by

$$\begin{aligned} \mathbf{u}_{\mathrm{in}1L} &= k_L^{-1}[+k_{Lx,} + k_y] \exp(+ik_{Lx,}x + ik_y y - i\omega t) \\ \mathbf{u}_{\mathrm{out}1L} &= R_{LL} k_L^{-1}[-k_{Lx,} + k_y] \exp(-ik_{Lx,}x + ik_y y - i\omega t) \\ \mathbf{u}_{\mathrm{out}1\,T} &= R_{TL} k_T^{-1}[+k_y + k_{Tx,}] \exp(-ik_{Tx,}x + ik_y y - i\omega t) \\ \mathbf{u}_{\mathrm{out}2L} &= T_{LL} k_L^{-1}[+k_{Lx,} + k_y] \exp(+ik_{Lx,}x + ik_y y - i\omega t) \\ \mathbf{u}_{\mathrm{out}12\,T} &= T_{TL} k_T^{-1}[-k_y + k_{Tx,}] \exp(+ik_{Tx,}x + ik_y y - i\omega t) \end{aligned} \tag{29}$$

where R_{LL}, R_{TL} are the reflection coefficients into longitudinal and transverse phonons, respectively, and T_{LL}, T_{TL} are the coefficients for transmission into the second medium.

To calculate the forces acting between the surfaces, we need to know the total amplitudes of the surface displacements, which are given by

$$\begin{aligned} u_{\mathrm{tot}1Lx} &= (1 - R_{LL}) k_L^{-1} k_{Lx} + R_{TL} k_T^{-1} k_y \\ u_{\mathrm{tot}2Lx} &= T_{LL} k_L^{-1} k_{Lx} + T_{TL} k_T^{-1} k_y \end{aligned} \tag{30}$$

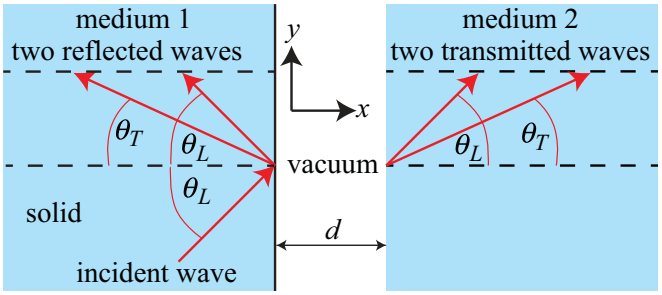

FIG. 3. An incident phonon (longitudinal in this instance) gives rise to two reflected phonons and two transmitted phonons of different polarizations. We assume that both surfaces are composed of the same isotropic homogeneous material.

Similarly, for an incident transverse phonon,

$$\begin{aligned}
\mathbf{u}_{\text{in1}T} &= k_T^{-1}[-k_y + k_{Tx,}]\exp(+ik_{Tx,}x + ik_y y - i\omega t)\\
\mathbf{u}_{\text{out1}L} &= R_{LT}k_L^{-1}[-k_{Lx,} + k_y]\exp(-ik_{Lx,}x + ik_y y - i\omega t)\\
\mathbf{u}_{\text{out1}T} &= R_{TT}k_T^{-1}[+k_y + k_{Tx,}]\exp(-ik_{Tx,}x + ik_y y - i\omega t)\\
\mathbf{u}_{\text{out2}L} &= T_{LT}k_L^{-1}[+k_{Lx,} + k_y]\exp(+ik_{Lx,}x + ik_y y - i\omega t)\\
\mathbf{u}_{\text{out2}T} &= T_{TT}k_T^{-1}[-k_y + k_{Tx,}]\exp(+ik_{Tx,}x + ik_y y - i\omega t)
\end{aligned} \tag{31}$$

From the formulae derived in the previous section, we can calculate the forces and match to the stress. The resulting expressions are somewhat complex and are given by the following formulae.

$$\begin{aligned}
T_{LL} &= \frac{2UV}{(V-W+X)^2-U^2},\ T_{TL} = ST_{LL}\\
R_{LL} &= \frac{-U^2-V^2+(W-X)^2}{(V-W+X)^2-U^2},\ R_{TL} = S[-1+R_{LL}]
\end{aligned} \tag{32}$$

and for the transverse incident phonons,

$$\begin{aligned}
T_{LT} &= \frac{-QU}{X^2+U^2-(V-W)^2}, \quad T_{TT} = ST_{LT},\\
R_{LT} &= \frac{-Q[X-V+W]}{X^2+U^2-(V-W)^2}, \quad R_{TT} = SR_{LT}+1
\end{aligned} \tag{33}$$

where,

$$\begin{aligned}
Q &= -4i\rho c_T^2 k_{Tx}k_y k_T^{-1},\\
S &= \frac{2k_{Lx}k_y k_T}{(k_y^2-k_{Tx}^2)k_L},\\
U &= \frac{C\pi}{4d^2}k_y^2 K_2(k_y d)k_L^{-1}k_{Lx}\frac{k_y^2+k_{Tx}^2}{k_y^2-k_{Tx}^2},\\
V &= i\rho c_T^2 k_L^{-1}(k_{Tx}^2-k_y^2),\\
W &= i\rho c_T^2 k_L^{-1}\frac{4k_y^2 k_{Tx}k_{Lx}}{(k_y^2-k_{Tx}^2)},\\
X &= \frac{C\pi}{2d^4}k_L^{-1}k_{Lx}\frac{k_y^2+k_{Tx}^2}{k_y^2-k_{Tx}^2}
\end{aligned} \tag{34}$$

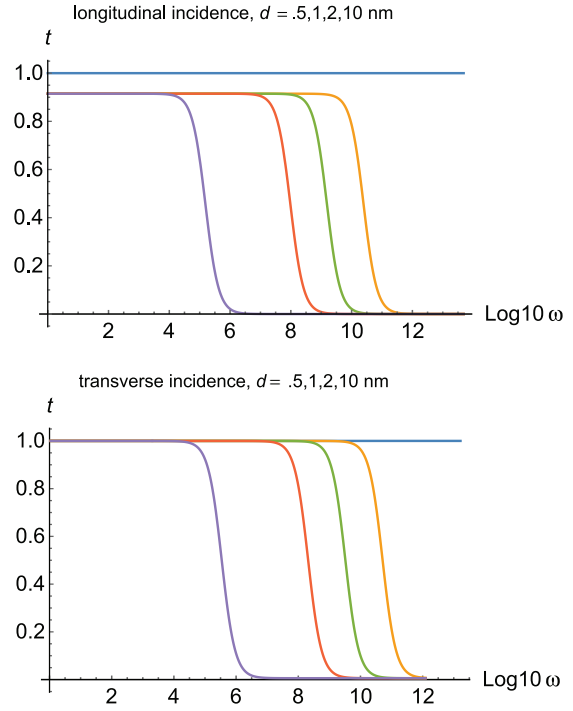

FIG. 4. Top: Fraction of longitundinal incident power transmitted between two slabs of gold plotted as a function of frequency in $\log_{10}$(radians per second). The spacing between the slabs is 0.5, 1.0, 2.0, and 10.0 nm, reading the curves from right to left. Bottom: As for top, but for transverse incident waves. The angle of incidence is $\pi/4$ radians.

Figure 4 shows the total power transmission coefficients for both longitudinal and transverse waves across a gap between two gold slabs. The parameters are as follows:

$$\begin{aligned}
C &= 34.76\times\pi^{-2}10^{-20}\text{J},\\
c_L &= 3240\,\text{ms}^{-1}\\
c_T &= 1200\,\text{ms}^{-1}\\
\rho &= 1.9280\times10^4\,\text{kgm}^{-3}\\
a &= 4.08\times10^{-10}\,\text{m}
\end{aligned} \tag{35}$$

where ρ is the density of gold, and a is the lattice constant. The value of C is taken from the Hamaker constant found in Pinchuk and Jiang [15].

For the most part, only a small fraction of the power is transmitted. This is because of the very large impedance mismatch across the gap due to the weak van der Waals force. However, for low frequencies, the transmission coefficient is near to unity. This comes about because, for a given amplitude of a phonon, the stress tensor is proportional to frequency, decreasing as the frequency is lowered. When the stress tensor is comparable to the van der Waals force acting across the gap, transmission will be high. Since the van der Waals force in this regime varies roughly as d^{-4}, where d is the slab separation, we expect the frequency of onset of maximum transmission to scale as d^{-4}. Figure 4 bears out this statement.

Figure 5 shows a contour plot of the transmitted power as a function of angle of incidence and frequency. Clearly, there is little variation with angle. We conclude that below a critical

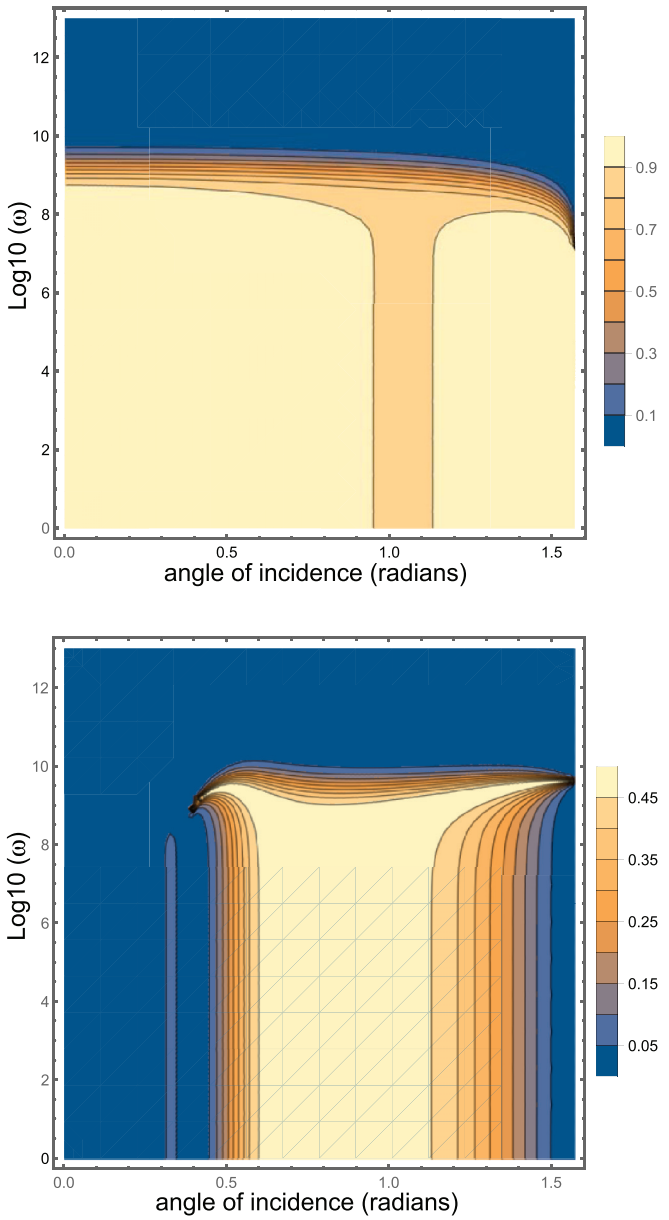

FIG. 5. Top contour plot of the fraction of longitudinal incident power transmitted between two slabs of gold showing frequency in $\log_{10}$(radians per second) on the vertical axis and angle of incidence in radians on the horizontal axis. Bottom: As for top, but for transverse incident waves. The spacing between the gold slabs in 1 nm.

frequency, the gap is highly transparent. The transition is broad in frequency, extending over one or two orders of magnitude about the central frequency. The transverse incident wave does not disturb the surface at normal incidence; therefore, transmission is zero, only rising at larger angles of incidence.

Note that high transmission occurs only at very low frequencies. Even for $d = 0.5$ nm, the transition is about 10^{10}rad s^{-1}. To put this in the current context, a thermal spectrum at $T = 0.076$ K would peak around this frequency. Therefore, when temperatures of around 300 K are considered, the picture is very different, with frequencies around 4×10^{13}rad s^{-1} being the relevant ones.

The high transparency at low frequencies has little impact on heat transmission, as we shall see in the next section. However, it may be relevant if near field heat conduction is being employed to cool a sample without mechanical contact. In fact, Fig. 4 shows that for low frequencies, there is very good mechanical contact, in so far as low-frequency noise is easily transmitted, and furthermore the lowest frequencies will be well transmitted even when the surfaces are quite far apart.

V. HEAT CONDUCTION ACROSS AN INTERFACE

We wish to use the transmission coefficients to calculate the heat transmitted across an interface. Each phonon state in the first medium will have an energy density of

$$\hbar\omega\left[\frac{1}{2}+\frac{1}{\exp(\hbar\omega/k_BT)-1}\right]L^{-3} \tag{36}$$

where $\hbar$ is Planck's constant, ω is the frequency of the phonon, k_B is Boltzmann's constant, T is the temperature in degrees Kelvin, and L is the dimension of the system. Since the zero point energy plays no role in heat transfer, we shall neglect it from this point onwards.

We shall assume that the $L\times L\times L$ box in which the phonons are confined obeys periodic boundary conditions so that the density of states in k space is $(L/2\pi)^3$. The heat flux per unit area in the direction of the surface is

$$\dot{Q}(T) = L^{-3}\sum_{\substack{k_{Lx}>0,\\ k_{Ly},k_{Ly}}} \frac{\hbar\omega_L}{\exp(\hbar\omega_L/k_BT)-1}\frac{c_L^2k_{Lx}}{\omega_L} + \frac{\hbar\omega_T}{\exp(\hbar\omega_T/k_BT)-1}\frac{c_T^2k_{Tx}}{\omega_T} \tag{37}$$

where the factor

$$\frac{c_L^2k_{Lx}}{\omega} = c_L\sin\theta \tag{38}$$

is the component of the phonon's velocity along the x axis. We assume linear dispersion so that the group and phase velocities coincide,

$$\omega_L = c_Lk_L, \qquad \omega_T = c_Tk_T \tag{39}$$

Although there are two transverse polarized waves, only the p-polarized transverse wave can cross a gap into a second solid.

If we now bring up a second surface, the probability of energy transmission into that second surface is $G_L$andG_T for the longitudinal and transverse phonon, respectively, and the heat flux is

$$\dot{Q}(T) = L^{-3}\sum_{\substack{k_{Lx}>0,\\ k_{Ly},k_{Ly}}} \frac{\hbar\omega_LG_L}{\exp(\hbar\omega_L/k_BT)-1}\frac{c_L^2k_{Lx}}{\omega_L} + \frac{\hbar\omega_TG_T}{\exp(\hbar\omega_T/k_BT)-1}\frac{c_T^2k_{Tx}}{\omega_T} \tag{40}$$

which we can rewrite in terms of integrals,

$$\dot{Q}(T) = \int\left[\frac{\hbar\omega_LG_Lc_L}{\exp(\hbar\omega_L/k_BT)-1} + \frac{\hbar\omega_TG_Tc_T}{\exp(\hbar\omega_T/k_BT)-1}\right]\frac{\sin2\theta}{8\pi^2}k^2dk \tag{41}$$

and we have recognized that the integrand is independent of the azimuthal orientation of the wave vector.

The fractions of these incident waves that are transmitted to the second surface are given by the transmission and reflection coefficients calculated in the previous section. We define

$$G_L = \frac{|T_{LL}|^2 \operatorname{Re} k_{Lx} c_L^2 + |T_{TL}|^2 \operatorname{Re} k_{Tx} c_T^2}{\operatorname{Re} k_{Lx} c_L^2},$$
$$G_T = \frac{|T_{LT}|^2 \operatorname{Re} k_{Lx} c_L^2 + |T_{TT}|^2 \operatorname{Re} k_{Tx} c_T^2}{\operatorname{Re} k_{Tx} c_T^2} \quad (42)$$

as the contributions of longitudinal and transverse waves, respectively. The factor $|T_{LL}|^2$ gives the intensity of the transmitted phonon field, and the power flow normal to the surface results from multiplying by the velocity normal to the surface,

$$c_L \cos\theta_L = c_L \frac{k_{Lx}}{k_L} = c_L^2 \frac{k_{Lx}}{\omega} \quad (43)$$

The common factor of ω cancels in Eq. (42).

Figure 6 shows the longitudinal and transverse contributions to the integral given in Eq. (41) for two gold slabs using the same parameters displayed in Eq. (34) and separated by 1 nm. Although the temperature is taken to be 300 K, with a typical frequency of

$$\omega = \frac{k_B T}{\hbar} \approx 4\times 10^{13} \text{rads}^{-1} \quad (44)$$

it is apparent from Fig. 6 that the major contributions to the integral come from much lower frequencies. This is due to the very steep dependence on frequency for the transmission coefficients as noted in section III. On the other hand, the high transmission at low frequencies does not contribute much to heat transfer. The integrand is trapped in a steep valley between the maximum density of states and the low-frequency rise in transmission.

Figure 7 shows the integrated heat flux from a gold surface at 300 K into a second surface for various separations together with a horizontal line showing the black body radiation. The phonon contribution declines very rapidly with increasing separation. The variation is not a simple power law as d^{-8} found in previous work, but accelerates at large distances.

The very strong dependence on separation dominates heat flow from phonons: Even large variations of other parameters can be nullified by a slight change in separation. Note that the weak black body flux is only equaled at a 1 nm separation. Although phonon flux rises dramatically beyond this point, the region is difficult for experiments and is where other forces begin to intrude.

TABLE I. Comparison of heat flux in watts per square meter for the spring model [2,3] and our model.

Spacing:	0.1 nm	1.0 nm	10 nm
Our model	6.20×10^{10}	8.80×10^{2}	7.00×10^{-7}
Spring model	6.46×10^{10}	5.35×10^{3}	5.03×10^{-5}

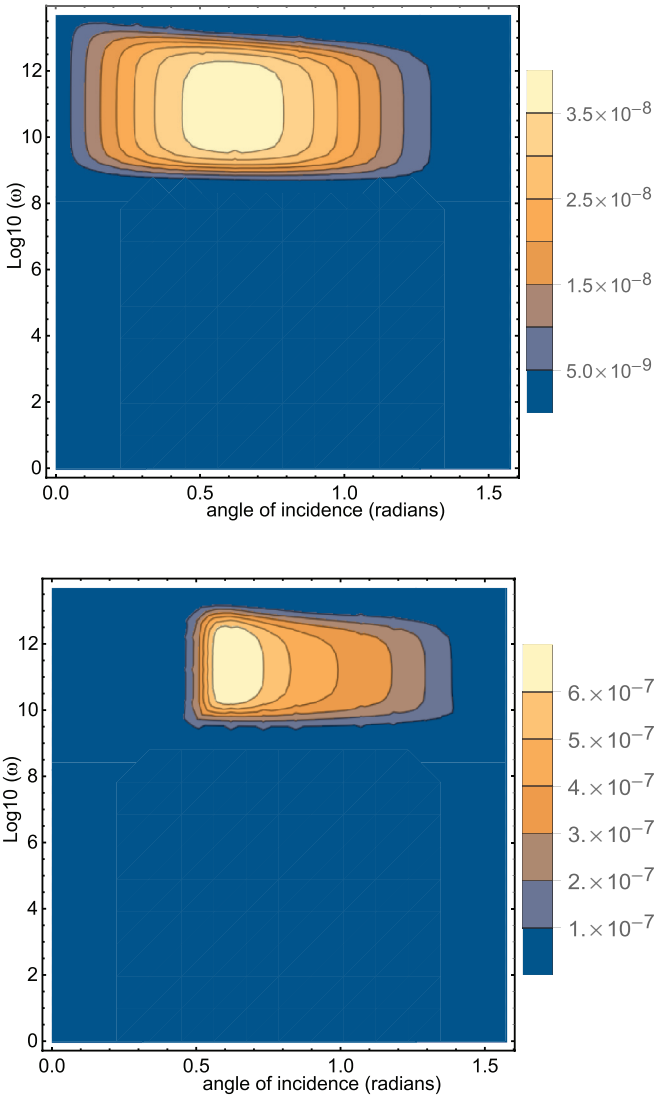

FIG. 6. Contour plots of the contributions to heat flow between two gold slabs at a temperature of 300 K, separated by 1 nm, as calculated in Eq. (41). Top: Longitudinal incident wave contributions; bottom: transverse incident wave contributions, showing frequency in $\log_{10}$(radians per second) on the vertical axis and angle of incidence in radians on the horizontal axis.

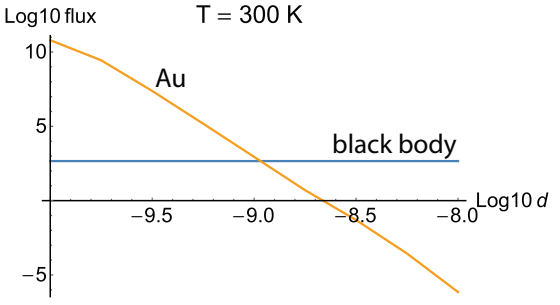

FIG. 7. $\log_{10}$ of the heat flux in watts per square meter between two gold slabs, at a temperature of 300 K, plotted against $\log_{10}$ of their separation in meters. The horizontal line represents black body radiation.

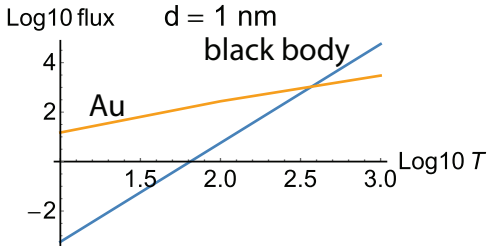

FIG. 8. $\log_{10}$ of the heat flux between two gold slabs, at a separation of 1 nm, plotted against $\log_{10}$ of the temperature. The steeper of the two lines represents black body radiation.

Our formula for the force exerted by a phonon on the opposite surface is given in Eq. (27) and if we take the limit,

$$\lim_{d\to 0} F_{x12} \mathrm{e}^{(ik_y y - i\omega t)} = -\frac{C\pi\delta_{2x}}{2d^4}\mathrm{e}^{(ik_y y - i\omega t)} \tag{45}$$

we retrieve the spring model with the d^{-4} scaling used in previous work [2,3], which in turn leads to a d^{-8} variation of the heat transfer with distance. We show the differences in Table I, which shows that when the surfaces are close, a d^{-4} force works well, but this soon breaks down at larger distances.

Figure 8 gives a different take on the results, showing $\log_{10}$ of the heat flux plotted against $\log_{10}$ of the temperature. The phonon contribution scales as T, in contrast to the T^4 scale of black body radiation. This is due to phonon transmission being heavily biased towards low frequencies, so that the temperature dependence in Eq. (41) reduces to the low-frequency limit. The curves cross at around 300 K, and the different scaling leads to phonons dominating at low temperatures.

VI. ELECTROSTATIC FORCES BETWEEN SURFACES

The van der Waals force is not the only long-range force acting between surfaces. If two surfaces are at different potentials, the capacitive charge will result in a force. This could arise from an externally imposed potential difference, or a work function difference if the two surfaces were composed of different metals. Even if the surfaces were both of gold, the microcrystalline structure of the surfaces would result in static potential differences between different areas, giving rise to a similar interaction to the van der Waals force, which is due to fluctuating dipoles. As an estimate of these effects, we consider the simplest case of a constant voltage difference between the two surfaces.

Two parallel conducting surfaces held at different voltages will support an electrostatic field acting between them, which in turn will exert an attractive force. If one of these surfaces experiences a periodic disturbance, such as a phonon might create, then the other surface will experience a periodic force that will transfer phononic energy from one surface to another.

Suppose surface 1 is held at voltage V_1, and surface 2 is held at voltage V_2. If the surfaces are separated by d, the voltage profile between the surfaces will have the form

$$V(x) = V_1 + (V_2 - V_1)x/d \tag{46}$$

and the field is

$$E = -\partial V/\partial x \ = -(V_2 - V_1)/d \tag{47}$$

Suppose that surface 1 has a periodic displacement of

$$u_{1x} = \delta_{1x}\exp(ik_y y - i\omega t) \tag{48}$$

where δ_{1x} is a real number supplied by the amplitudes of incident and reflected waves in medium 1. We require that the potential takes the value V_1 on this corrugated surface. Introducing perturbations of the same periodicity into the potential gives

$$\begin{aligned} V(x) &= V_1 + (V_2 - V_1)x/d \\ &\quad + [v_- e^{-k_y x} + v_+ e^{+k_y x}]e^{+ik_y y - i\omega t} \end{aligned} \tag{49}$$

The additional terms obey Laplace's equation, as any electrostatic field must do, and by adjusting v_-, v_+, we can also satisfy the boundary conditions. First, we require that surface 2 is at a constant potential V_2

$$v_- e^{-k_y d} + v_+ e^{+k_y d} = 0 \tag{50}$$

and next that surface 1 is at a constant potential of V_1,

$$\begin{aligned} V_1 &= V[\delta_{1x}\exp(ik_y y - i\omega t)] \\ &= V_1 + (V_2 - V_1)[\delta_{1x} e^{ik_y y - i\omega t}]d^{-1} \\ &\quad + \begin{bmatrix} v_- e^{-k_y[\delta_{1x}\exp(ik_y y - i\omega t)]} \\ + v_+ e^{+k_y[\delta_{1x}\exp(ik_y y - i\omega t)]} \end{bmatrix} e^{+ik_y y - i\omega t} \end{aligned} \tag{51}$$

We assume that phonon frequencies are low, so that magnetic fields do not play a role; i.e., we make the quasistatic approximation. If we assume that the phonon displacements, δ_{1x}, are very small, then

$$\begin{aligned} V_1 &= V[\delta_{1x} e^{ik_y y - i\omega t}] \\ &\approx V_1 + (V_2 - V_1)[\delta_{1x} e^{ik_y y - i\omega t}]d^{-1} \\ &\quad + [v_- + v_+]e^{+ik_y y - i\omega t} \end{aligned} \tag{52}$$

Hence,

$$0 = (V_2 - V_1)\delta_{1x}/d \ + [v_- + v_+] \tag{53}$$

Using Eq. (50) and Eq. (53),

$$\begin{aligned} v_- &= -\frac{e^{+k_y d}}{e^{+k_y d} - e^{-k_y d}}\frac{\delta_{1x}}{d}(V_2 - V_1) \\ v_+ &= -v_- e^{-2k_y d} = +\frac{e^{-k_y d}}{e^{+k_y d} - e^{-k_y d}}\frac{\delta_{1x}}{d}(V_2 - V_1) \end{aligned} \tag{54}$$

The electric field normal to surface 2 is

$$\begin{aligned} E_x(d) &= -\frac{\partial V}{\partial x}(x = d) \\ &= -(V_2 - V_1)/d + 2k_y v_- e^{-k_y d + ik_y y - i\omega t} \end{aligned} \tag{55}$$

and hence from Maxwell's stress tensor,

$$F_{x21} = \frac{1}{2}\varepsilon_0\frac{(V_2 - V_1)^2}{d^2}\left[1 - \frac{2\delta_{1x}k_y}{\sinh(k_y d)}e^{+ik_y y - i\omega t}\right] \tag{56}$$

Note the asymptotic scaling as d^{-3} compared to d^{-4} for the van der Waals case.

The electrostatic contributions to phonon heat transfer are shown in Fig. 9 for a 1 V potential difference between the gold slabs. Otherwise, the parameters are the same as in Figs. 7 and 8. Note the different dependence on separation shown in the top figure, with the flux tailing off much more slowly

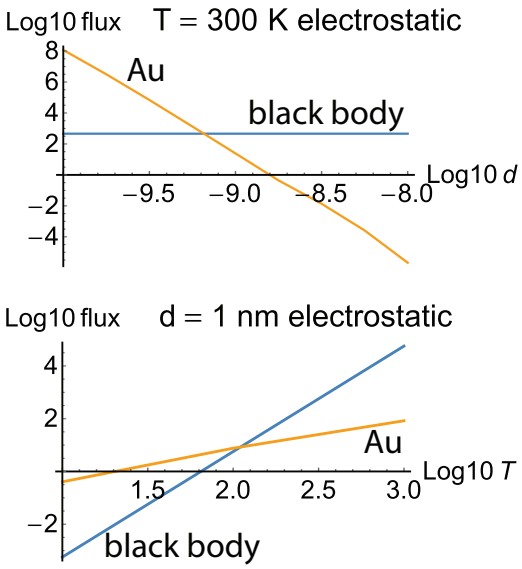

FIG. 9. Compare with Figs. 7 and 8, but with electrostatic forces substituted for the van der Waals force. A voltage difference of 1 V between the slabs of gold was assumed.

compared to the case of van der Waals forces. In the lower figure, the temperature dependence shows the same scaling proportional to T as did the van der Waals case, again due to the low-frequency biasing from the phonon transmission coefficient.

Overall, the magnitude of the forces is not very different from the van der Waals case. This means that distinguishing the two experimentally will be difficult, as indeed was the case when experiments tried to measure van der Waals forces directly.

VII. COMPARISON WITH NEAR FIELD HEAT FLUX AND CONCLUSIONS

In previous work [6], heat transfer through fluctuations in the near field was studied. If the gap between the two surfaces is much less than the relevant wavelengths at the temperature of the bodies, then the heat flux is given by

$$\dot{Q}(T,d) = \frac{4}{\pi^2}\int_0^\infty\int_0^\infty d\omega k_y dk_y \frac{\hbar\omega}{\exp(\hbar\omega/k_BT)-1} \times\left[\frac{(\mathrm{Im}\,R_p)^2 e^{-2k_y d}}{\left|1-R_p^2 e^{-2k_y d}\right|^2}+\frac{(\mathrm{Im}\,R_s)^2 e^{-2k_y d}}{\left|1-R_s^2 e^{-2k_y d}\right|^2}\right] \quad (57)$$

where we have assumed all distances are small compared to the free space wavelength of radiation at temperature T, and hence they work in the electrostatic approximation. This is an excellent approximation for all length scales considered in this paper. R_p and R_s are the surface reflectivities for s- and p-polarized fields respectively.

$$R_p = \frac{\varepsilon k_x - k_x'}{\varepsilon k_x + k_x'}, \quad R_s = \frac{\mu k_x - k_x'}{\mu k_x + k_x'} = \frac{k_x - k_x'}{k_x + k_x'} \quad (58)$$

and,

$$k_x = i\sqrt{k_y^2 - \omega^2/c_0^2}\,, \quad k_x' = i\sqrt{k_y^2 - \varepsilon\omega^2/c_0^2} \quad (59)$$

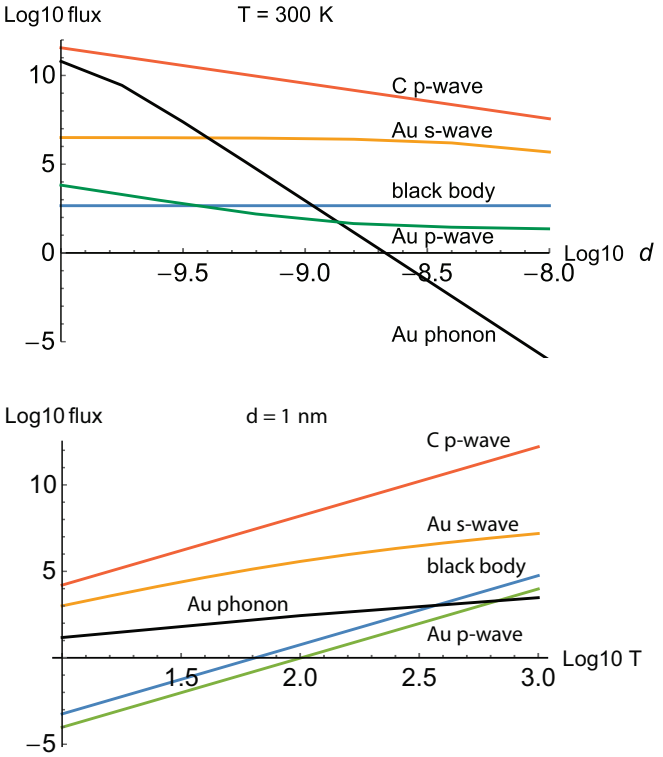

FIG. 10. Comparison of the heat flux due to several processes. Top: Flux plotted at $T = 300$ K against $\log_{10}$ of the spacing between the two slabs. The red curve is for the near field mechanism in amorphous carbon, the black curve is for the van der Waals phonon mechanism, the green curve is for the near field p-wave mechanism in gold, the orange curve is for the near field s-wave mechanism in gold, and the blue curve is for black body radiation. Bottom: The same as above, but plotted against $\log_{10}$ of the temperature at a constant space of $d = 1$nm.

where k_x, k_x' are components of the wave vectors *in vacuo* and in the medium, respectively. For highly conducting materials such as gold, the s-polarized contribution dominates. It operates through magneto-inductive coupling of electrical currents in opposing surfaces. For more resistive materials such as amorphous carbon, the p-polarized contribution dominates.

Figure 10 compares various mechanisms: the phonon tunneling mechanism for gold, the near field mechanisms for gold and amorphous carbon, and black body radiation. We assumed the following form for the dielectric function of gold,

$$\varepsilon_{Au} = 1 - \frac{\omega_p^2}{\omega^2 + i\omega\nu} \quad (60)$$

where for gold, following Chapuis *et al.* [16],

$$\omega_p = 1.71\times10^{16}, \quad \nu = 4.05\times10^{13} \quad (61)$$

and for amorphous carbon,

$$\varepsilon_C = 1 + \frac{i\sigma}{\varepsilon_0\omega} \quad (62)$$

where a typical conductivity is given by,

$$\sigma = 2\times10^3 \quad (63)$$

The most striking contrast between phonon tunneling via van der Waals forces and near field tunneling consists of huge differences between the conductivities of various materials. This is well illustrated by Fig. 10, where amorphous carbon and gold have near field heat transfer values that differ by several orders of magnitude. This same observation also applies to the far field radiation, which is massively reduced for a highly reflecting surface such as gold.

In contrast, the van der Waals mechanism is much more consistent. As Israelachvili observed, the Hamaker constant, which controls these forces, differs from one material to another by less than a factor of ten. Therefore, although we have chosen gold as an example of phonon heat transfer, results for other materials will not be qualitatively different.

Another striking difference is the dependence of these forces on distance and on temperature. The near field p-polarized flux scales as d^{-2} and so rapidly outpaces the van der Waals–driven phonon contributions with increasing distance. However, as has been observed previously, the s-polarized contribution is almost independent of d, provided that

$$d < \sqrt{\frac{\hbar\varepsilon_0 c_0^2}{\sigma k_B T}} \tag{64}$$

If this condition holds, the cutoff for integration over the wave vector in Eq. (57) is imposed by the expression for $\mathrm{Im}\, R_s(k_y)$, which happens at

$$k_y \approx \sqrt{\frac{\sigma k_B T}{\hbar\varepsilon_0 c_0^2}} \tag{65}$$

so there is no dependence on distance. For gold at 300 K, the critical distance is around 2×10^{-8}m.

The phonon contributions fall off very rapidly with d in our model, even more rapidly than the d^{-8} scaling found in the spring model of phonons [2,3]. Even the electrostatic-mediated phonon contributions scale as d^{-6}, but all are eventually beaten by the near field flux. This drastic dependence on d means that phonon flux is very short range indeed and hard to distinguish from the covalent forces arising when two surfaces touch.

Materials such as amorphous carbon produce the most powerful heat transfer at distances beyond the range of chemical bonding but still provide significant heat flow. In amorphous carbon, the impedance is well matched to maximizing the flow of heat, as discussed in an earlier paper [6].

The temperature dependence of the phonon flux scales as T, in contrast to the near field p-flux and black body flux, both of which scale as T^4.

VIII. TRANSPORT BY RAYLEIGH MODES

The Rayleigh modes are surface states bound just below the transverse modes in frequency. They are populated by scattering of energy out of the extended modes, and they transfer energy to an opposing surface by tunneling across the gap. The ratio of these two rates determines the contribution to heat transport. We shall use the splitting of the Rayleigh modes as they hybridize across the surface to calculate the tunneling rate.

We model the modes on either side of the surface as two coupled harmonic oscillators

$$\omega^2\begin{bmatrix} a_1 \\ a_2 \end{bmatrix} - \begin{bmatrix} \Omega^2(\omega,T) \\ 0 \end{bmatrix} = \begin{bmatrix} \omega_{k_R}^2 - i\omega_{k_R}\delta & \omega_{k_R}\gamma \\ \omega_{k_R}\gamma^* & \omega_{k_R}^2 - i\omega_{k_R}\delta \end{bmatrix}\begin{bmatrix} a_1 \\ a_2 \end{bmatrix} \tag{66}$$

where a_1, a_2 are the amplitudes of the mode on surface 1 and surface 2, respectively, ω_{k_R} is the frequency of the unperturbed mode with wave vector k_R, and δ is the broadening of the modes due to coupling to the extended modes and is responsible both for feeding heat into the mode on surface 1 and removing heat from the mode on surface 2. If $\delta = 0$, as assumed in our calculations in previous sections, no heat gets into the Rayleigh modes, and their contribution to heat flow is eliminated. The value of δ will vary from sample to sample, but estimates of broadening of the extended modes give a typical value of 1 meV in the middle of the spectrum, tending to zero at zero frequency [17]. We shall assume

$$\delta(k_y) \approx 1.97\times10^2\times k_y \ \mathrm{rad\,s^{-1}} \tag{67}$$

which is consistent with this estimate.

$\Omega^2(\omega,T)$ represents a heat source (assumed to be the extended modes) and ensures thermal equilibrium of the uncoupled first surface if we choose

$$|\Omega^2(\omega,T)|^2 = \frac{\omega_0^2\delta}{2\pi}\frac{1}{\exp(\hbar\omega/k_BT)-1} \tag{68}$$

We shall assume that in the absence of coupling, the second surface is at $T = 0$.

Here, γ couples the modes on the two surfaces and results in a splitting of the modes,

$$\omega^2 = \omega_{k_R}^2 - i\omega_{k_R} \pm \omega_{k_R}|\gamma| \tag{69}$$

and hence $|\gamma|$ can be found from our previous formalism: The denominators in Eq. (33) are zero at the Rayleigh mode frequencies.

From Eq. (66) and we calculate

$$|a_2|^2 = \frac{|\Omega^2(\omega,T)|^2}{4}\left|\frac{2\omega_{k_R}|\gamma|}{\left(\omega^2-\omega_{k_R}^2+i\omega_{k_R}\delta\right)^2-\omega_{k_R}^2|\gamma|^2}\right|^2 \tag{70}$$

Upon integrating over all frequencies ω, we end up with an expression for the flow of heat into the second surface, being proportional to the broadening, to be given by:

$$\dot{Q}_R = \int_0^\infty \frac{\hbar\omega_{k_R}}{\exp\left(\hbar\omega_{k_R}/k_BT\right)-1}\frac{\delta|\gamma|^2k_Rdk_R}{16\pi(|\gamma|^2+\delta^2)} \tag{71}$$

For realistic distances of separation $|\gamma| \ll \delta$,

$$\dot{Q}_R \approx \int_0^\infty \frac{\hbar\omega_{k_R}}{\exp\left(\hbar\omega_{k_R}/k_BT\right)-1}\frac{|\gamma|^2}{\delta}\frac{k_Rdk_R}{16\pi} \tag{72}$$

In this limit, increasing δ decreases the heat flow, and since we assume an otherwise perfect surface and substrate, our estimate is likely to be too large.

Performing the integration gives the graph shown in Fig. 11.

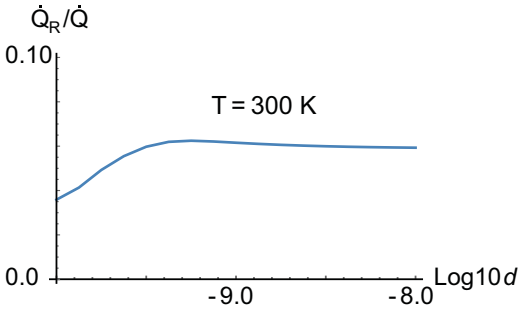

FIG. 11. Heat flux due to the Rayleigh modes calculated for gold at $T = 300$ K and divided by the other near field contributions shown in Fig. 10.

We conclude that, at least for our example of gold, the contribution of Rayleigh modes to heat flow is just a few percent of the total contribution.

ACKNOWLEDGMENTS

R.V.C. and J.B.P. gratefully acknowledge support from the Engineering and Physical Sciences Research Council (EPSRC) programme, Grant No. EP/L024926/1, and the Leverhulme Trust. This project has received funding from the European Union's Horizon 2020 Research and Innovation programme under the Marie Sklodowska-Curie Grant Agreement No. 702525. J.B.P. also thanks the Gordon and Betty Moore Foundation for support Contract No. 3385.

[1] B. N. J. Persson, A. I. Volokitin, and H. Ueba, J. Phys.: Condens. Matter **23**, 045009 (2011).
[2] B. V. Budaev and D. B. Bogy, Appl. Phys. Lett. **99**, 053109 (2011).
[3] Y. Ezzahri and K. Joulain, Phys. Rev. B **90**, 115433 (2014).
[4] V. Chiloyan, J. Garg, K. Esfarjani, and G. Chen, Nat. Commun. **6**, 6755 (2015).
[5] D. Polder and M. Van Hove, Phys. Rev. B **4**, 3303 (1971).
[6] J. B. Pendry, J. Phys.: Condens. Matter **11**, 6621 (1999).
[7] A. I. Volokitin and B. N. J. Persson, Phys. Rev. B **63**, 205404 (2001).
[8] D. P. Sellan, E. S. Landry, K. Sasihithlu, A. Narayanaswamy, A. J. H. McGaughey, and C. H. Amon, Phys. Rev. B **85**, 024118 (2012).
[9] B. V. Budaev and D. B. Bogy, Z. Angew. Math. Phys. **62**, 1143 (2011).
[10] L. D. Landau and E. M. Lifshitz, *Theory of Elasticity* (Pergamon, New York, 1975).
[11] J. N. Israelachvili, *Intermolecular and Surface Forces*, 3rd ed. (Academic Press, London, 2011).
[12] M. Abramowitz and I. A. Stegun, *Handbook of Mathematical Functions* (Dover, Mineola, NY, 1970).
[13] P. M. Echenique and J. B. Pendry, J. Phys. C **9**, 3183 (1976).
[14] P. M. Echenique and J. B. Pendry, Phys. Rev. Lett. **37**, 561 (1976).
[15] P. Pinchuk and K. Jiang, Proc. SPIE **9549**, 95491J (2015).
[16] P. O. Chapuis, S. Volz, C. Henkel, K. Joulain, and J. J. Greffet, Phys. Rev. B **77**, 035431 (2008).
[17] Xiaoli Tang and B. Fultz, Phys. Rev. B **84**, 054303 (2011).